Molecular Microbiology (2015) 96(4), 694–707 ■
doi:10.1111/mmi.12964
First published online 6 March 2015

A high-throughput screen for ligand binding reveals the specificities of three amino acid chemoreceptors from *Pseudomonas syringae* pv. *actinidiae*

James L. O. McKellar,† Jordan J. Minnell† and Monica L. Gerth*
Department of Biochemistry, University of Otago, PO Box 56, Dunedin 9054, New Zealand.

Summary

Chemoreceptors play a central role in chemotaxis, allowing bacteria to detect chemical gradients and bias their swimming behavior in order to navigate toward favorable environments. The genome of the kiwifruit pathogen, *Pseudomonas syringae* pv. *actinidiae* (*Psa*) strain NZ-V13 encodes 43 predicted chemoreceptors, none of which has been characterized. We developed a high-throughput fluorescence-based thermal shift assay for identifying the signal molecules that are recognized by a given chemoreceptor ligand binding domain (LBD). Using this assay, we characterized the ligand binding profiles of three *Psa* homologs of the *P. aeruginosa* PAO1 amino acid chemoreceptors PctA, PctB and PctC. Each recombinant LBD was screened against 95 potential ligands. The three *Psa* homologs, named *pscA*, *pscB* and *pscC* (*Psa* chemoreceptors A, B and C) bound 3, 10 and 3 amino acids respectively. In each case, their binding profiles were distinct from their *P. aeruginosa* PAO1 homologs. Notably, *Psa* PscA-LBD only bound the acidic amino acids L-aspartate, D-aspartate and L-glutamate, whereas *P. aeruginosa* PctA-LBD binds all of the L-proteinogenic amino acids except for L-aspartate and L-glutamate. A combination of homology modeling, site-directed mutagenesis and functional screening identified a single amino acid residue in the *Psa* PscA-LBD (Ala146) that is critically important for determining its narrow specificity.

Introduction

Chemotaxis allows motile bacteria to sense changes in their chemical environment and navigate toward favorable conditions (Adler, 1966). The major components of bacterial chemotaxis systems include methyl-accepting chemotaxis proteins (MCPs), the sensor histidine kinase CheA and the response regulator CheY (Hazelbauer *et al.*, 2008). MCPs, also called chemoreceptors, are the key sensory components in the chemotaxis signaling pathway. Chemoreceptors bind specific extracellular chemicals, which can be either attractants or repellants for the bacterium (Adler, 1969; Tso and Adler, 1974; Rahman *et al.*, 2014). Upon ligand binding, chemoreceptors transduce a signal through the CheAY two-component system, which ultimately controls flagellar rotation and bacterial motility (Hazelbauer *et al.*, 2008).

Historically, the chemotaxis system of *Escherichia coli* has been the primary framework for understanding chemoreceptor structure and function [reviewed in Wadhams and Armitage (2004)]. *E. coli* has four chemoreceptors (Tar, Tsr, Trg and Tap) that mediate chemotaxis primarily in response to specific amino acids, dipeptides, sugars and pyrimidines. Each chemoreceptor has three distinct structural and functional modules: a ligand binding domain (LBD), a HAMP (histidine kinases, adenylyl cyclases, methyl-accepting chemotaxis proteins and phosphatases) domain and a signaling domain. The N-terminal LBD is responsible for sensing environmental stimuli, either directly or via an additional periplasmic binding protein. The HAMP domain acts as the signal relay, and the signaling domain transmits the signal to the chemotactic machinery. For a given chemotactic bacterium, the repertoire and specificities of its chemoreceptor proteins determine the molecules to which it responds.

In contrast to *E. coli* and other related enterobacteria, the chemotaxis systems of soil and aquatic microorganisms are poorly understood. Genome sequencing has revealed that environmental bacteria typically have complex chemosensory systems, with 20–60 *mcp* genes per genome (Lacal *et al.*, 2010b). Although most bacterial chemoreceptors (~74%) appear to share the same overall three-domain topology as the *E. coli* proteins, the sequence diversity of their LBDs is extremely high (Wuichet and Zhulin, 2003; Lacal *et al.*, 2010b). As a result, most of what they bind is not known. For example, even in the relatively well-studied pathogen *Pseudomonas aerugi-*

Accepted 5 February, 2015. *For correspondence. E-mail monica.gerth@otago.ac.nz; Tel. +64 3 479 7836; Fax +64 3 479 7866.
†These authors contributed equally to this work.

nosa PAO1, only 13 of its 26 putative MCPs have been characterized (Alvarez-Ortega and Harwood, 2007; Kato *et al.*, 2008; Rico-Jimenez *et al.*, 2013). A recent in-depth study of the amino acid chemoreceptors from *P. aeruginosa* PAO1 emphasized that the basis of chemosensing in Pseudomonads can be drastically different from that of the enterobacteria (Rico-Jimenez *et al.*, 2013). Both *E. coli* and *P. aeruginosa* PAO1 possess chemoreceptors for sensing amino acids; however, the LBDs that mediate this response are completely unrelated. The periplasmic LBDs of *E. coli* chemoreceptors (Tar and Tsr) consist of anti-parallel four-helix bundles of approximately 160 amino acids (Tajima *et al.*, 2011). The LBDs of the amino acid receptors from *P. aeruginosa* (PctA, PctB and PctC) are larger (approximately 250 amino acids) and are predicted to adopt a mixed α/β, double PDC (PhoQ/DcuS/CitA) fold. This appears to be a case of parallel evolution, where different receptor types have evolved to mediate chemotaxis to the same class of compounds (i.e. amino acids).

It remains a major challenge to understand how a bacterium senses (and thus responds to) its environmental niche. A related, methodological question is: how might we identify the signal molecules that are recognized by a given chemoreceptor? For bacteria with large numbers of chemoreceptors, functional redundancy and masking by other behaviors (such as aerotaxis) have hampered attempts to link individual chemoreceptor proteins to their cognate ligands.

We are interested in defining the ligand binding profiles of chemoreceptors from the plant pathogen, *Pseudomonas syringae* pv. *actinidiae* (*Psa*). *Psa* is a major global pathogen of kiwifruit, causing severe economic losses in countries such as Italy and New Zealand, where kiwifruit is a major crop (Scortichini *et al.*, 2012). *Psa* invades plant tissues through natural openings and lesions on the plant surface, resulting in wilting, cankers and plant death (Scortichini *et al.*, 2012). It is known that chemotaxis is critical for many pathogenic species to colonize and invade a host. For example, many plant-associated microbes are specifically attracted to host plant exudates such as amino acids, organic acids and sugars (de Weert *et al.*, 2002; Yao and Allen, 2006). However, the chemoreceptors that mediate this behavior are largely unknown. Genome sequencing of a virulent strain of *Psa* isolated in New Zealand (strain NZ-V13) encodes 43 predicted MCPs (McCann *et al.*, 2013). Although this is significantly more than the number of MCPs found in the better characterized chemosensory systems of *P. aeruginosa* (26 predicted MCPs) or *P. putida* (27 predicted MCPs), it is similar to that of other *P. syringae* strains such as *P. syringae* pv. *phaseolicola* 1448A (44 predicted MCPs) or *P. syringae* pv. *tomato* str. DC3000 (46 predicted MCPs) (Kato *et al.*, 2008; Winsor *et al.*, 2011; Parales *et al.*, 2013).

In order to shed light on the function of its chemoreceptors, and how they may differ from the receptors of other *Pseudomonas* species, we have begun to characterize the *Psa* chemoreceptor repertoire. We have developed and validated a new and generalizable high-throughput method for rapidly screening recombinant LBDs against a library of potential ligands. Using this assay, we have characterized the ligand binding profiles of three *Psa* LBDs that are homologous to the *P. aeruginosa* PAO1 amino acid sensors, PctA, PctB and PctC. Each of the homologous *Psa* LBDs was found to bind a distinct subset of amino acids and unexpectedly, their binding profiles were also distinct from their *P. aeruginosa* PAO1 homologs. Further investigation using a combination of homology modeling, site-directed mutagenesis and isothermal titration calorimetry identified a key residue involved in determining the ligand specificity of *Psa* PscA.

Results

Validation of a high-throughput, fluorescence-based thermal shift assay to detect ligand binding

Fluorescence-based thermal shift (FTS) assays have been used for more than a decade to characterize the ligand binding specificities of a variety of proteins (Pantoliano *et al.*, 2001; Lo *et al.*, 2004; Niesen *et al.*, 2007; Giuliani *et al.*, 2008). FTS assays are based on the principle that most ligands stabilize proteins upon binding, causing an increase in the melting temperature of the protein (Niesen *et al.*, 2007; Cimmperman *et al.*, 2008). The melting temperature is measured by an increase in the fluorescence of a dye with affinity for hydrophobic parts of the protein (e.g. SYPRO Orange), which are exposed as the protein unfolds. FTS assays can be performed in 96-well format using readily available real-time PCR instrumentation. Though not all proteins are amenable to FTS measurements (e.g. large multi-domain proteins tend not to exhibit distinct phase transitions during thermal denaturation; and some ligands may bind primarily to the unfolded state of the protein), the overall simplicity and general applicability of FTS assays make this technique a powerful tool for identifying protein–ligand interactions. Here, we have developed an FTS assay for rapid screening of chemoreceptor LBDs against hundreds of different potential ligands.

We have used FTS assays to screen recombinantly produced LBDs against the compounds in Biolog Phenotype Microarray (PM) plates. PM plates are a commercially available library of potential metabolic substrates (e.g. various carbon, nitrogen, phosphorus and sulfur sources) (Bochner *et al.*, 2001). Each 96-well PM plate contains 95 different chemicals and an empty control well. PM plates are designed to be used in conjunction with a tetrazolium indicator dye to characterize the metabolic capabilities of

microbial species and strains. However, for use in our FTS assays, the compounds were resuspended in water, generating a library of potential ligands for high-throughput screening. Aliquots of each ligand solution could then be added to the purified LBD and SYPRO Orange dye, distributed in the wells of a 96-well polymerase chain reaction (PCR) plate. Fluorescence intensity was measured as the temperature was raised. The ability of a molecule to stabilize the protein during its thermal unfolding could be quantified by its thermal shift (ΔT_m): the difference in the protein unfolding temperature in the presence and absence of ligand.

To validate this method, we first screened the PctA-LBD from *P. aeruginosa* PAO1 (*Pae* PctA-LBD), which is a well-characterized amino acid LBD. Previous work using isothermal titration calorimetry (ITC) showed that *Pae* PctA-LBD directly binds 17 amino acids *in vitro*; no binding was detected for L-aspartate, L-glutamate or L-glutamine (Rico-Jimenez *et al.*, 2013). For comparison with these data, we performed FTS assays of the purified *Pae* PctA-LBD with the Biolog PM3B microplate, which includes all 20 proteinogenic L-amino acids. The LBD domain of *Pae* PctA (residues Asn30-Ala278) was expressed with an N-terminal His_6 tag, as described previously (Rico-Jimenez *et al.*, 2013). The *Pae*-PctA-LBD was overexpressed, purified using immobilized metal affinity chromatography and subjected to FTS assays.

Overall, the ligand binding profile of the *Pae* PctA-LBD obtained by our FTS assay was consistent with the previously published ITC data. In the absence of ligand, *Pae* PctA-LBD displayed a temperature midpoint of unfolding (T_m) of 62.0 ± 0.2°C. Of the amino acids known to bind *Pae* PctA-LBD directly, 15 resulted in temperature shifts (ΔT_m values) of > 2°C, whereas two (L-cysteine and L-histidine) produced smaller temperature shifts of 1.7°C ± 0.01 and 1.2 ± 0.3°C respectively (Fig. 1A). On the other hand, the three amino acids that *Pae* PctA-LBD had previously been reported not to bind (L-aspartate, L-glutamate and L-glutamine) yielded ΔT_m values of 0.15 ± 0.07°C, 0.19 ± 0.16°C and 1.0 ± 0.11°C (Fig. 1A). Furthermore, Biolog plate PM3B contains D-alanine, D-glutamate, putrescine and the dipeptides L-ala-L-gln and L-ala-L-gly, all of which had previously been shown not to be ligands of *Pae* PctA-LBD (Rico-Jimenez *et al.*, 2013). Our screen confirmed these results while also identifying another 66 compounds that do not stabilize *Pae* PctA-LBD (Table S1). Our thermal shift assays also revealed an additional six nonproteinogenic amino acids that are ligands of *Pae* PctA-LBD: L-citrulline; L-homoserine; L-ornithine; D,L-α-amino-N-butyric acid; D,L-α-amino-caprylic acid and α-amino-N-valeric acid (Table S1). We confirmed that PctA is the sole chemoreceptor responsible for chemoattraction to four of these ligands (L-citrulline L-ornithine, D,L-α-amino-caprylic acid and α-amino-N-valeric acid) using quantitative capillary chemotaxis assays to compare *P. aeruginosa* PAO1 with an unmarked *pctA* deletion strain, *P. aeruginosa* PAO1 Δ*pctA* (Fig. S1).

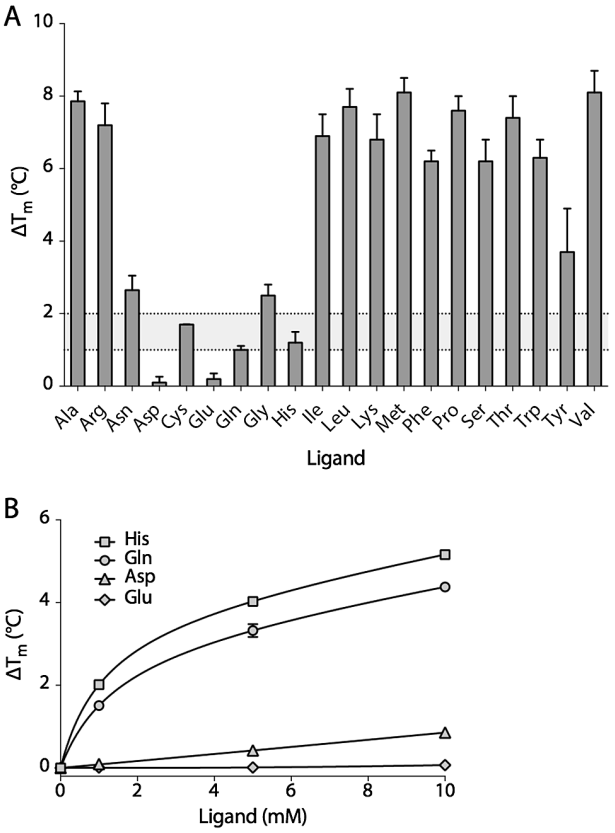

Fig. 1. A. Fluorescence-based thermal shift assays of *Pae* PctA-LBD with the 20 proteinogenic L-amino acids. Each histogram indicates the ΔT_m, calculated as the T_m in the presence of ligand minus the T_m in the absence of ligand. A positive ΔT_m indicates stabilization of the protein in the presence of the ligand. B. Rescreening *Pae* PctA-LBD with increasing concentrations of binding and nonbinding ligands. L-histidine, a cognate ligand of *Pae* PctA-LBD, stabilizes the protein in a concentration dependent manner. In contrast, increasing concentrations of a nonbinding compound (L-glutamate or L-aspartate) does not have a stabilizing effect. Data in (A) and (B) are the means and standard deviations from three experiments. If not visible, the error bars are contained within the symbol.

The thermal stability of a protein is proportional to the concentration of the ligand that it binds (Niesen *et al.*, 2007). In order to resolve the ambiguity around LBD:ligand pairs that gave small but significant ΔT_m values, we rescreened *Pae* PctA-LBD with increasing concentrations of selected ligands (Fig. 1B). As predicted, L-histidine, which is known to bind *Pae* PctA-LBD with a dissociation constant (K_D) of 28 μM (Rico-Jimenez *et al.*, 2013), stabilized the protein in a concentration dependent manner. Conversely, L-aspartate and L-glutamate did not bind *Pae* PctA-LBD in previously conducted ITC experiments (Rico-Jimenez *et al.*, 2013), and increasing the concentrations of these compounds did not significantly increase

the thermal stability of the protein in our assay (Fig. 1B). In the case of L-glutamine, our FTS screen showed a marginal increase in T_m (1.0 ± 0.1°C). It has been reported that L-glutamine is not a ligand of *Pae* PctA-LBD (Rico-Jimenez *et al*., 2013). However, the unfolding temperature of the protein was shifted to higher temperatures with increasing concentrations of L-glutamine (Fig. 1B), suggesting that L-glutamine may indeed be recognized by *Pae* PctA-LBD. To investigate these conflicting results, we used ITC to quantitatively assess binding. Microcalorimetric titration of *Pae* PctA-LBD with L-glutamine resulted in exothermic heat signals that dissipated into heats of dilution (Fig. S2). The affinity derived from the binding curve yielded a K_D of 90 ± 8 μM. Although the affinity of *Pae* PctA-LBD for L-glutamine was weak, the value is within the range reported for other bacterial chemoreceptor–ligand interactions (Lacal *et al*., 2010a; Rico-Jimenez *et al*., 2013; Webb *et al*., 2014). Thus, our ITC results confirmed the high-throughput FTS assay and demonstrated the direct binding of L-glutamine to *Pae* PctA-LBD.

Together, these experiments established the tractability of using Biolog PM plates as compound libraries for high-throughput FTS assays. Based on the results of our proof-of-principle study with the *Pae* PctA-LBD, in subsequent analyses, we considered a chemical to be a binding ligand if it yielded an average ΔT_m of 2°C or greater under our standard assay conditions. This is a similar threshold to those used in previous FTS studies (Giuliani *et al*., 2008; Krishna *et al*., 2013). For compounds with stabilizing effects in the range of 1–2°C, LBDs were rescreened in the presence of increasing concentrations of the potential ligand to confirm binding. An average ΔT_m of < 1°C was considered to represent no ligand binding by the LBD that was under consideration.

Predicted chemoreceptor periplasmic sensory domains of Psa

The *Psa* NZ-V13 genome (McCann *et al*., 2013) is predicted to encode 43 methyl-accepting chemotaxis proteins. We analyzed the sequence of each putative *Psa* chemoreceptor to determine its predicted membrane topology using TOPCONS (Bernsel *et al*., 2009) and to identify any conserved domains using CD-Search (Marchler-Bauer and Bryant, 2004). Based on this analysis, 33 of the 43 putative chemoreceptors had identifiable LBDs; that is, they contain a periplasmic region flanked by transmembrane helices, and they have identifiable HAMP and signaling domains (Table 1). Chemoreceptor LBDs typically fall into one of two distinct clusters: cluster I receptors of approximately 150 amino acids; or cluster II receptors of approximately 250 amino acids (Lacal *et al*., 2010b). The LBDs of *Psa* follow this trend, with 32 of the 33 predicted LBDs identified as belonging to either cluster I or II; one predicted LBD has an unusually small LBD of only 29 amino acids (Table 1). The structure of each LBD was also predicted using the Phyre2 protein fold recognition server (Kelley and Sternberg, 2009). The results are shown in Table 1. Four-helix bundles were predicted to be the most prevalent LBDs in *Psa*, accounting for 12 of the 33 predicted structures. In contrast, six of the LBDs were so dissimilar to any protein of solved structure that Phyre2 was unable to model them at all. None of the predicted *Psa* chemoreceptors have been previously studied.

Pseudomonas aeruginosa PAO1 contains three amino acid sensing chemoreceptors (PctA, PctB and PctC). The pairwise amino acid sequence identities between the LBDs of these three proteins are 68% (PctA and PctB), 54% (PctA and PctC) and 45% (PctB and PctC). The *P. aeruginosa* PAO1 PctA, PctB and PctC-LBDs all display quite different ligand binding specificities. As discussed above, PctA binds 18 proteinogenic amino acids. On the other hand, PctB binds five (L-glutamine tightly, and L-arginine, L-lysine, L-alanine and L-methionine more weakly), and PctC binds only three (L-histidine, L-proline and γ-aminobutyrate). In general, the low sequence conservation among the LBDs of chemoreceptors makes it difficult to identify ligand-specific signatures. However, when we used each of the three *P. aeruginosa* PAO1 *pct* genes to query the *Psa* NZ-V13 genome using BLAST, we got the same hits in all three searches: *Psa* loci Psa_14525, Psa_08785 and Psa_18055. The LBDs encoded by these *Psa* genes follow a similar pattern of sequence identities as their *P. aeruginosa* homologs, with the products of Psa_14525 and Psa_08785 being more closely related to each other (41% amino acid identity) than they are to Psa_18055 (19% and 23% identity respectively). Each of the three *Psa* LBDs was also predicted to adopt a double PDC-like fold (Table 1), modeled on an uncharacterized chemoreceptor LBD from *Vibrio cholerae*, which had L-alanine bound (PDB ID 3C8C). This is the same structure that was used previously to generate a model of *Pae* PctA-LBD (Rico-Jimenez *et al*., 2013). Thus, based on our bioinformatics analysis, we hypothesized that *Psa* senses amino acids using three chemoreceptors that are functionally equivalent to *P. aeruginosa*: PctA, PctB and PctC. However, based on sequence alone, it is not possible to predict the ligand specificities of the three *Psa* chemoreceptors, therefore high-throughput FTS assays were conducted.

Ligand binding profiles of Psa_14525, Psa_08785 and Psa_18055

We used our high-throughput FTS assay to characterize the ligand specificities of the putative PctA, PctB and PctC homologs from *Psa*. The three predicted LBDs were cloned, expressed and purified. Yields of the purified

Table 1. Identification of putative chemoreceptor LBDs from *Psa* NZ-V13 and the prediction of their structures.

Locus tag	Sensor domain[a]	Cluster	Conserved domains	Top PDB hit[b]	% Identity	% Coverage[c]	Predicted structure
Psa_14495	44–73	–	None identified	No hit	–	–	–
Psa_04165	33–190	I	4HB_MCP_1	3VA9	12	75	Four-helix bundle
Psa_06330	38–195	I	4HB_MCP_1	2ASR	13	61	Four-helix bundle
Psa_07150	31–189	I	4HB_MCP_1	3VA9	13	76	Four-helix bundle
Psa_08120	34–190	I	4HB_MCP_1	3VA9	9	75	Four-helix bundle
Psa_08545	32–190	I	4HB_MCP_1	No hit	–	–	–
Psa_08575	34–194	I	4HB_MCP_1	No hit	–	–	–
Psa_08870	33–188	I	4HB_MCP_1	3VA9	14	76	Four-helix bundle
Psa_13100	31–188	I	Cache_2	4K08	43	91	PAS-like
Psa_13805	35–141	I	None identified	No hit	–	–	–
Psa_16920	32–188	I	4HB_MCP_1	3VA9	16	77	Four-helix bundle
Psa_19595	33–190	I	4HB_MCP_1	3VA9	18	75	Four-helix bundle
Psa_19640	23–172	I	4HB_MCP_1	3VA9	13	81	Four-helix bundle
Psa_20080	31–206	I	Cache_2	3UB9	22	93	PAS-like
Psa_20455	33–191	I	4HB_MCP_1	3VA9	11	74	Four-helix bundle
Psa_20470	34–195	I	4HB_MCP_1	1VLT	15	53	Four-helix bundle
Psa_23495	33–188	I	4HB_MCP_1	3VA9	13	78	Four-helix bundle
Psa_26265	33–190	I	4HB_MCP_1	3VA9	12	77	Four-helix bundle
Psa_00575	33–308	II	Cache_3	3C8C	13	84	Double PDC-like
Psa_08780	35–289	II	None identified	2YFA	44	92	HBM domain
Psa_08785	**30–273**	**II**	**Cache_1**	**3C8C**	**28**	**96**	**Double PDC-like**
Psa_08985	42–332	II	None identified	4AKK	16	90	NIT domain
Psa_13180	36–291	II	None identified	2YFA	17	89	HBM domain
Psa_14525	**31–276**	**II**	**Cache_1**	**3C8C**	**26**	**96**	**Double PDC-like**
Psa_17695	37–283	II	4HB_MCP_1	2YFA	25	92	HBM domain
Psa_17955	28–310	II	None identified	3I9Y	11	71	TorS-like
Psa_18055	**28–293**	**II**	**Cache_1**	**3C8C**	**21**	**89**	**Double PDC-like**
Psa_19395	32–311	II	Cache_1	3LIB	15	93	Double PDC-like
Psa_24210	26–280	II	None identified	No hit	–	–	–
Psa_24710	37–309	II	None identified	No hit	–	–	–
Psa_25320	39–286	II	PilJ	2YFA	25	92	HBM domain
Psa_25325	39–295	II	None identified	2YFA	22	90	HBM domain
Psa_27745	41–323	II	None identified	4AKK	13	92	NIT domain

The three sensor domains characterized in this work are shown in bold font.
a. Numbers given are the amino acid residues that comprise the sensor domain, which were identified as the regions between predicted transmembrane segments using TOPCONS.
b. It was considered as no hit when the coverage of the top Phyre2 model was below 60%.
c. Coverage is the percentage of sequence modeled with > 97% confidence by the single highest scoring template.

LBDs were typically 20–30 mg per liter of culture medium. The proteins were > 95% pure and migrated as expected based on their respective subunit masses on SDS-PAGE gels (Fig. S3). To determine their ligand binding profiles, each recombinant LBD was screened against the compounds in Biolog plate PM3. The results of these assays are shown in Fig. 2. Potential ligands that resulted in marginal stabilizing effects (ΔT_m values of 1–2°C) were rescreened using FTS assays with increasing ligand concentration, to verify binding (Fig. S4).

The Psa_14525-LBD was found to be specific for acidic amino acids (Fig. 2A). In the absence of ligands, Psa_14525-LBD had a T_m of 44.0 ± 0.1°C. Of the 95 potential ligands that were screened, L-aspartate, L-glutamate and D-aspartate resulted in dramatic stabilization of the protein, with ΔT_m values of 11.2°C, 8.5°C and 10.4°C respectively. This specificity for acidic and D-amino acids was unexpected, as none of the homologous amino acid chemoreceptors from *P. aeruginosa* PAO1 are able to recognize any of these ligands (Rico-Jimenez *et al.*, 2013).

For the LBD encoded by the open reading frame (ORF) Psa_08785, the unfolding temperature of the protein without ligand was 42.3 ± 0.1°C. In comparison with the Psa_14525-LBD, this LBD had a broader ligand binding profile (Figs 2B and S4A). The FTS screens yielded 10 ligands with significant ΔT_m values. The largest shifts were with the polar uncharged amino acids L-glutamine and L-asparagine (both ΔT_ms > 7°C). The *Psa* 08785-LBD was also stabilized, albeit to a lesser extent, by binding L-alanine, L-isoleucine, L-leucine, L-methionine, L-phenylalanine, L-serine, L-tryptophan and the non-proteinogenic amino acid L-homoserine (Fig. 2B). *Psa* 08785-LBD specifically bound L-amino acids. We were unable to detect an increase in the T_m with any of the D-amino acids that were screened, including the D-forms of asparagine, alanine and serine. This confirmed our

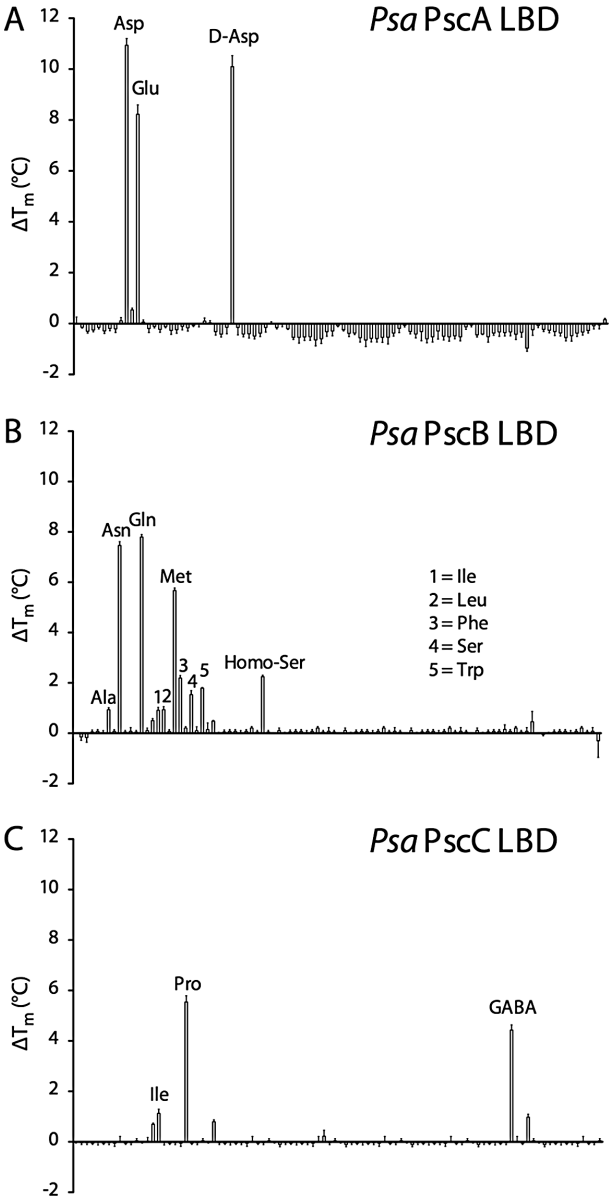

Fig. 2. The ligand binding profiles of the *Psa* (A) PscA, (B) PscB, and (C) PscC LBDs. Each LBD was screened against Biolog plate PM3B. The histograms indicate the T_m shifts between the no ligand control and 95 potential ligands. The ligands that bind and significantly stabilize the respective LBDs are labeled. All amino acids are the L-form unless otherwise indicated. Values shown are the mean ± SD ($n = 3$).

assignment of Psa_08785 as the homolog of *P. aeruginosa* PctB, because *Pae* PctB is the sole chemoreceptor for L-glutamine and it binds this amino acid with high affinity while it is also capable of binding four other amino acids (the Psa_08785 ligands L-methionine and L-alanine, as well as L-arginine and L-lysine) with significantly lower affinities (Rico-Jimenez *et al.*, 2013).

The T_m of the *Psa* 18055-LBD in the absence of ligand was similar to the other LBDs (40.1 ± 0.1°C). As shown in Fig. 2C, large T_m shifts, indicative of ligand binding, were observed with L-proline (ΔT_m 5.5 ± 0.2°C) and the nonproteogenic amino acid γ-aminobutyrate (GABA) (ΔT_m 4.4 ± 0.2°C). The *Psa* 18055-LBD is also stabilized by L-isoleucine (Fig. S4B). Overall, this binding profile is similar to that of PctC from *P. aeruginosa* PAO1, which recognizes L-proline, L-histidine and GABA (Rico-Jimenez *et al.*, 2013).

Based on their sequences and ligand binding profiles, the Psa_14525, Psa_08785 and Psa_18055 proteins were designated PscA, PscB and PscC (*Psa* chemoreceptors A, B and C) respectively.

The affinities of Psa PscA-LBD for acidic and D-amino acids

The difference between the ligand binding profiles of *Psa* PscA-LBD and its homolog from *P. aeruginosa* PAO1 is striking. *Psa* PscA-LBD is extremely specific – only binding aspartate (L- and D-stereoisomers) and L-glutamate – while *Pae* PctA-LBD binds all of the proteinogenic L-amino acids except for aspartate and glutamate. To enable comparison with the previously characterized PctA-LBD from *P. aeruginosa* PAO1 (Rico-Jimenez *et al.*, 2013), isothermal titration calorimetry was used to quantify the affinities of *Psa* PscA-LBD for its ligands. As shown in Fig. 3, titration of *Psa* PscA-LBD with either L-aspartate or L-glutamate resulted in large exothermic heat signals. *Psa* PscA-LBD showed the highest affinity for L-aspartate, with a K_D value of 6.1 ± 0.9 μM. It bound L-glutamate with a lower affinity ($K_D = 27 \pm 6$ μM). The direct binding of D-aspartate to *Psa* PscA-LBD was also confirmed by ITC (Fig. 3C and Fig. S5); however, the binding did not fit to the one-site model. Instead, the isotherms fit best to a two-site binding model. The two-site model predicts a high affinity site with a K_D of 2.3 ± 1.0 μM and a low affinity site with a K_D of 19 ± 6 μM.

Psa PscA is the sole receptor that detects L-aspartate, L-glutamate and D-aspartate

The above studies show that *Psa* PscA-LBD binds three ligands *in vitro*. We next wanted to assess the contribution of the *Psa* PscA receptor in chemotaxis toward these ligands. We used quantitative capillary assays to measure the chemotactic response of both the wild-type *Psa* and *Psa* Δ*pscA* strains toward L-aspartate, L-glutamate and D-aspartate. The wild-type *Psa* strain showed a clear chemotactic response toward each of these amino acids (Fig. 4). In contrast, no significant chemoattraction was observed for the *Psa* Δ*pscA* strain (Fig. 4). These results suggest that PscA is the only *Psa* chemoreceptor for chemoattraction toward L-aspartate, L-glutamate and D-aspartate.

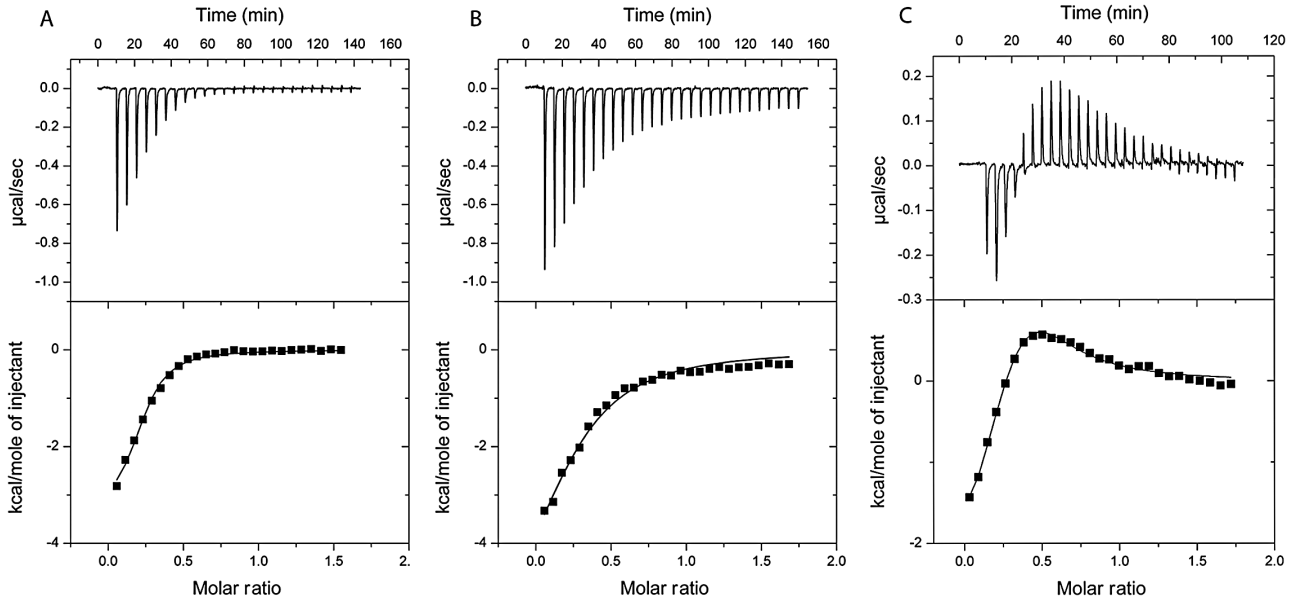

Fig. 3. Representative isothermal titration calorimetry data of *Psa* PscA-LBD with (A) L-aspartate, (B) L-glutamate and (C) D-aspartate. The upper panels show raw titration data; the lower panels are the integrated and dilution corrected peak areas of the titration data. For the titrations *Psa* PscA-LBD was at 120 µM, and the ligands were at 1 mM.

The role of residue 146 in the ligand specificity of Psa PscA-LBD

To identify residues that contribute to the unexpected ligand specificity of the *Psa* PscA-LBD, we submitted the LBD sequence to the Phyre2 protein structure prediction server (Kelley and Sternberg, 2009). The best model was based on the structure of an LBD from an uncharacterized *V. cholerae* chemoreceptor (McpN, residues 63–300, PDB code 3C8C) (Fig. 5A). Phyre2 could use the *V. cholerae* LBD to model 96% of the residues in the *Psa* PscA-LBD at > 99% confidence. The *V. cholerae* McpN-LBD crystallizes as a homodimer, where each monomer has a double PDC fold (Fig. 5A). In each monomer, there are six key amino acid residues that comprise the ligand binding pocket and make direct contacts with the L-alanine ligand (Fig. 5A and B). A structure-based alignment showed that the equivalent residues in five of these six positions are identical in the *Pae* PctA and *Psa* PscA-LBDs (Fig. S6); the only position in the ligand binding sites of the *Pae* PctA and *Psa* PscA-LBDs that differs is residue 146. It is an alanine in the *Psa* PscA-LBD (Fig. 5C), whereas it is an aspartate in the *P. aeruginosa* (and *V. cholerae*) LBD. In the *V. cholerae* structure, the side chain carboxyl group of this aspartate residue forms a hydrogen bond with the amino group of the alanine ligand (Fig. 5B). In the homology model of *Psa* PscA-LBD (Fig. 5C), this hydrogen bond is abolished.

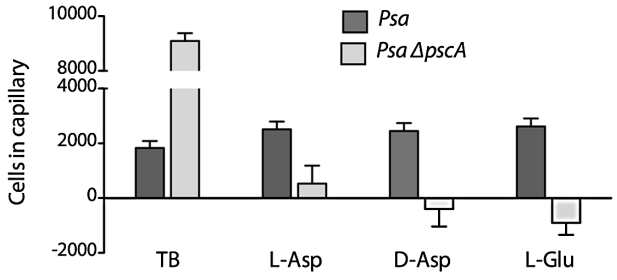

Fig. 4. Quantitative capillary chemotaxis assay of wild-type *Psa* and *Psa* Δ*pscA* to L-aspartate, D-aspartate and L-glutamate (each at 1 mM). The data have been normalized to a buffer only control by subtracting the average number of cells that accumulated in capillaries containing only the chemotaxis buffer. Also shown is the positive control response to tryptone broth (TB). The results are the means of at least three independent experiments, and error bars indicate standard errors.

The potential role of residue 146 in the ligand specificity of *Psa* PscA-LBD was not clear based on the homology model; therefore, to explore the role of this residue further we used site-directed mutagenesis to produce an Ala146Asp variant of *Psa* PscA-LBD. The recombinant LBD was purified (Fig. S3), and we then performed FTS assays against the compounds in Biolog plate PM3B. In the absence of ligand, the A146D variant displayed an increased stability ($T_m = 50.0 \pm 0.1°C$) compared with the wild-type protein ($T_m = 44.0 \pm 0.1°C$). The A146D variant also displayed a dramatically broadened ligand binding profile, with significant ΔT_m values detected for 15 amino acids: L-alanine, L-aspartate, L-cysteine, L-glutamine, L-isoleucine, L-leucine, L-methionine, L-phenylalanine, L-serine, L-threonine, L-tryptophan, L-valine and the non-

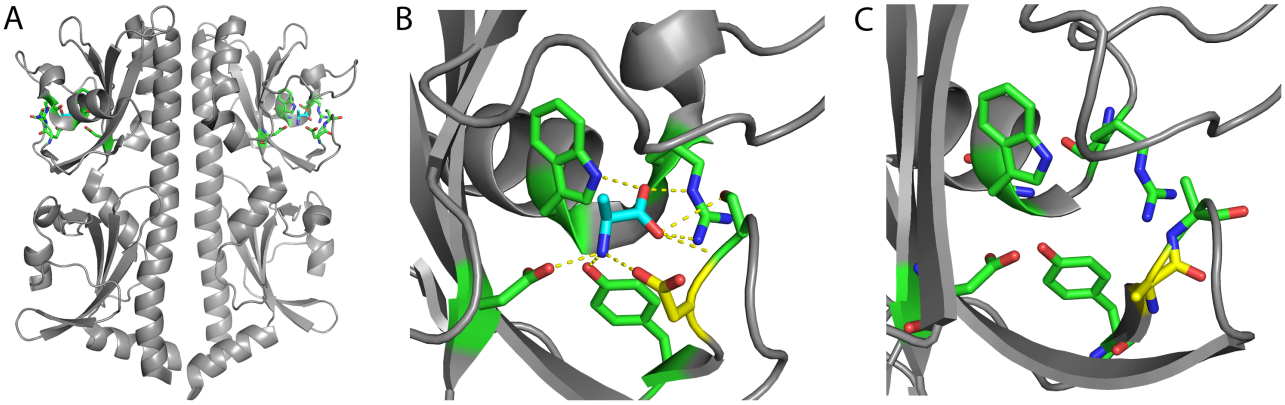

Fig. 5. Identification of PscA residues involved in ligand binding, using the structure of *V. cholerae* McpN (PDB ID 3C8C) as a model.
A. The structure of the *V. cholerae* McpN-LBD dimer. Each monomer adopts a double PDC-like fold. The alanine ligand is shown as sticks with blue backbone. The residues predicted to interact with the alanine ligand are shown as sticks with green backbone.
B. A close up view of the McpN ligand binding pocket. Six residues make contact with the alanine ligand: R152, W154, Y170, D172, S173 and D201. The residue D172, which corresponds to A146 in *Psa* PscA, is shown in yellow.
C. A homology model of *Psa* PscA-LBD, based on the *V. cholerae* McpN structure, generated using Phyre2. Residues predicted to interact with the ligand are shown as sticks (green backbone), except for the residue targeted for mutagenesis (A146), which is shown in yellow.

proteinogenic amino acids D,L-α-amino-N-butyric acid, D,L-α-amino-caprylic acid and α-amino-N-valeric acid (Fig. 6 and Fig. S4C). The A146D variant retained the ability to bind L-aspartate; however, the ability to bind L-glutamate was abolished. The A146D mutation also conferred a new ability to bind amino acids with hydrophobic side chains.

Next, we performed ITC measurements to quantify the affinities of the A146D variant for L-aspartate and two of the new, hydrophobic amino acid ligands (L-leucine and L-methionine). The A146D-LBD was also titrated against L-glutamate to confirm the absence of binding. The results of the titrations are shown in Fig. 7. Compared with the wild-type *Psa* PscA-LBD, the binding of L-aspartate was characterized by a fivefold lower affinity ($K_D = 170 \pm 10$ μM). The affinity of the A146D mutant for L-methionine was similar to L-aspartate, with a $K_D = 210 \pm 40$ μM. The microcalorimetric titrations confirmed that the A146D variant does also bind L-leucine, but the affinity for this ligand is weak, with a K_D of 470 ± 110 μM. Interestingly, the binding was exothermic for L-aspartate but endothermic for the more hydrophobic amino acids, L-methionine and L-leucine. In general, a positive enthalpy (endothermic process) suggests that hydrophobic effects play a substantial role in binding, whereas a negative enthalpy (exothermic process) indicates an interaction based primarily on hydrogen bonding. Therefore, our ITC results suggest that the ligands may bind via different mechanisms.

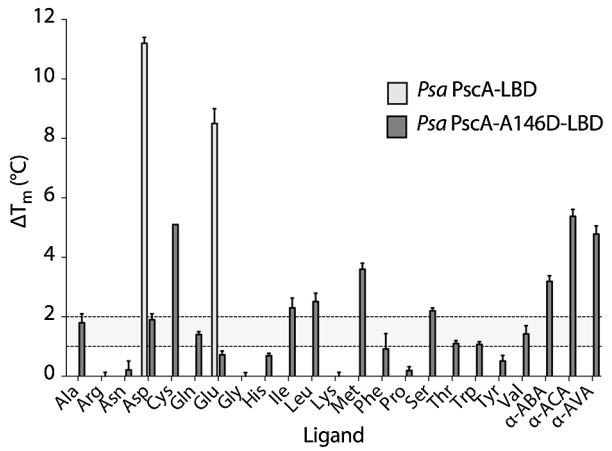

Fig. 6. The A146D mutation broadens the amino acid binding range of *Psa* PscA-LBD. Results from fluorescence-based thermal shift assays of the wild-type *Psa* PscA-LBD and the A146D mutant with the ligands from the Biolog PM3B plate. For clarity, only the histograms for the proteinogenic L-amino acid ligands, and the other ligands from the PM3B plate that stabilize the respective LBDs are shown. ABA = D, L-α-amino-N-butyric acid; ACA = D, L-α-amino-caprylic acid and AVA = α-amino-N-valeric acid. Values shown are the mean ± SD ($n = 3$).

Discussion

Genome sequencing has revealed an enormous diversity of LBDs in bacterial chemotaxis systems (Krell *et al.*, 2011). Despite the abundance of chemoreceptors, relatively little is known regarding the sensory specificity of LBDs, or the contributions of individual chemoreceptors to the lifestyles of bacteria. Traditional genetic approaches are hampered by two problems, particularly in bacteria that possess large numbers of chemoreceptors. First, it can be difficult to obtain mutants that are deficient in chemotaxis to a specific compound because of functional redundancy; that is, many bacteria possess multiple chemoreceptors that mediate responses to the same

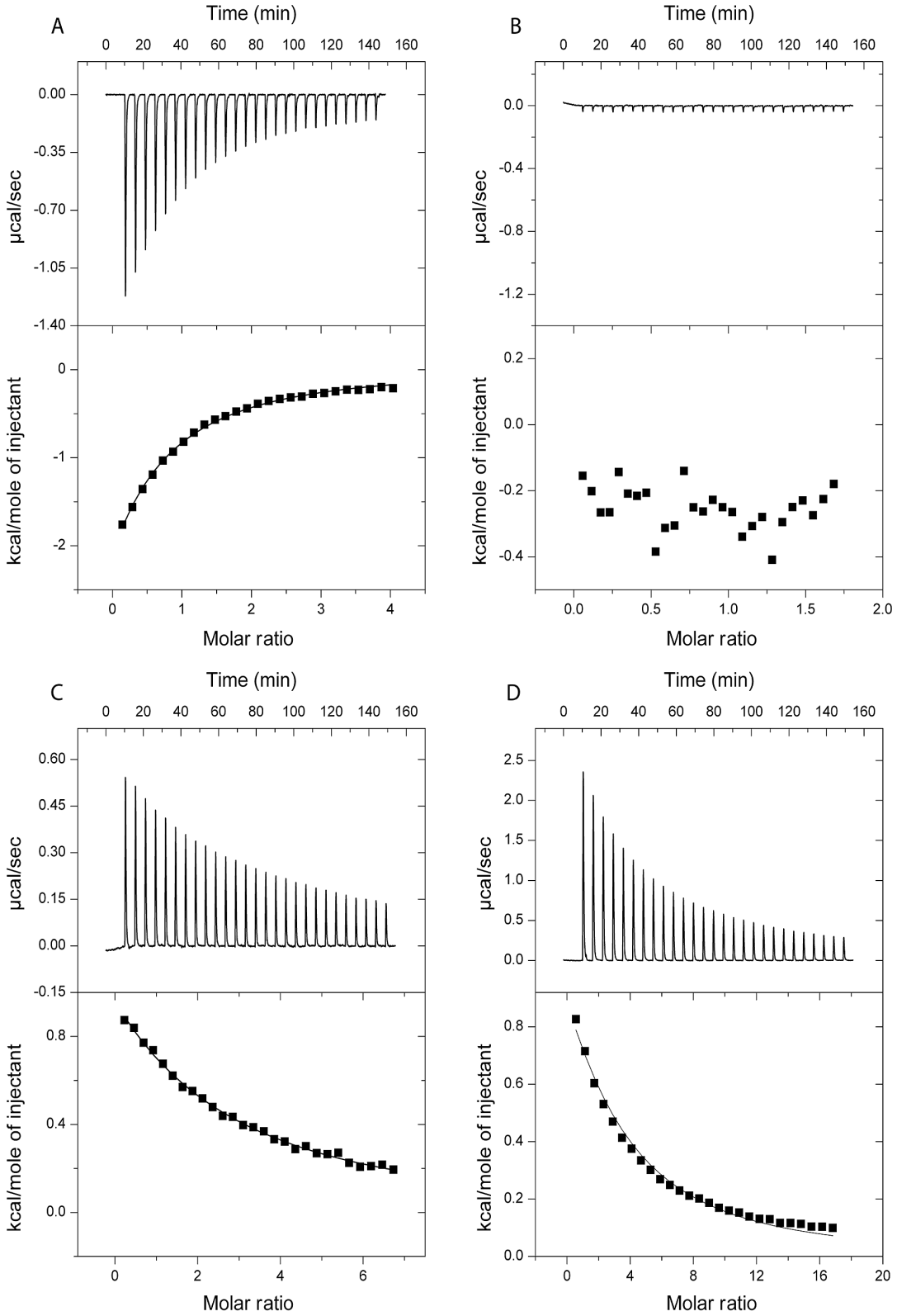

Fig. 7. Representative isothermal titration calorimetry of the *Psa* PscA A146D-LBD with different ligands. The upper panels show raw titration data; the lower panels are the integrated and dilution corrected peak areas of the titration data. Titration of: (A) 120 µM *Psa* PscA A146D-LBD with 1 mM L-aspartate; (B) 60 µM *Psa* PscA A146D-LBD with 0.5 mM L-glutamate; (C) 60 µM *Psa* PscA A146D-LBD with 2 mM L-methionine; and (D) 120 µM *Psa* PscA A146D-LBD with 10 mM L-leucine.

ligand. Second, aerotaxis can mask a chemotaxis phenotype. In addition, the potential range of environmental and metabolic molecules that a bacterium may respond to is enormous, which adds combinatorial complexity to the problem of understanding chemosensory systems from environmental bacteria such as *Pseudomonas*.

In the first part of this study, we evaluated the utility of FTS assays for determining the ligand binding profiles of chemoreceptor LBDs. The strength of FTS assays is the ability to rapidly survey large numbers of potential ligands against an LBD of unknown function. A purified LBD can be screened against 95 potential ligands in less than 2 h. To simplify and standardize our screen, we used Biolog PM plates as the sources of our ligands.

To begin, we tested our assay with a well-characterized LBD from *P. aeruginosa* PAO1. Overall, we observed an excellent correlation with the previous ligand binding assignments of the *Pae* PctA-LBD. All 17 of the previously identified ligands produced significant T_m shifts in our assays (Fig. 1A). However, in contrast to previous work (Rico-Jimenez *et al*., 2013), our FTS assay also identified L-glutamine as a potential ligand for *Pae* PctA-LBD. We confirmed this response using both compound titration (Fig. 1B) and ITC (Fig. S2). Although this result is surprising, it is not inconsistent with the known chemotactic responses of *P. aeruginosa* PAO1 to L-glutamine (Taguchi *et al*., 1997; Rico-Jimenez *et al*., 2013). Rico-Jimenez *et al*. showed clearly that PctB – and not PctA – is the sole chemoreceptor for the attractant response of *P. aeruginosa* PAO1 to L-glutamine; however, they also observed a repellent response to L-glutamine that was independent of PctB (Rico-Jimenez *et al*., 2013). They suggested that an additional, unknown chemoreceptor mediates this response. Our results suggest that PctA is the chemoreceptor that mediates the repellent response of *P. aeruginosa* PAO1 to L-glutamine, although further studies will be required to confirm this hypothesis.

We anticipate that our high-throughput screen will be of general utility for revealing the ligands detected by any chemoreceptor LBD that can be heterologously expressed and purified. Though it is possible that a recombinant LBD may not exhibit the same binding properties as the full-length protein, it has been shown previously that molecular determinants for ligand recognition typically reside in the LBD and that full-length MCPs and recombinant LBDs can bind with similar affinities and stoichiometries (Glekas *et al*., 2010; 2012; Tajima *et al*., 2011). Although we have validated our screen with the PM3B microplate, the full set of PM plates 1–10 contains ~900 different chemicals, including known bacterial carbon, nitrogen, phosphorus and sulfur sources. PM plates 11–20 contain another 240 chemicals that are common bacterial toxins (and therefore potential chemorepellents), including antibiotics and metals. Together, these provide a tractable, affordable and quick way to gain qualitative data on molecules that are, or are not, bound by a given LBD. However, quantitative techniques such as ITC are still required to determine the relative affinities of the ligands that are identified. Our data suggest that FTS assays should not be used to rank ligands, as ΔT_m values are not always a reflection of relative affinities. For example, L-leucine and L-methionine resulted in similar thermal shifts (ΔT_m values ~8°C) with the *Pae* PctA-LBD (Fig. 1), although their measured affinities differ by over two orders of magnitude [K_D values of 116 and 0.91 μM respectively; Rico-Jimenez *et al*. (2013)]. The magnitude of the T_m shift observed when a compound binds an LBD is dependent on the contributions of both enthalpy and entropy; therefore, ligands with a range of different affinities can give rise to the same change in T_m (Niesen *et al*., 2007).

Our FTS assay allowed us to rapidly interrogate the binding profiles of three predicted amino acid sensing LBDs from *Psa*. Combined, the *Psa* PscA-LBD (encoded at locus Psa_14525), the PscB-LBD (Psa_08785) and the PscC-LBD (Psa_18055) proteins recognize 13 of the 20 proteinogenic L-amino acids. Each LBD detects a subset of amino acids, and each has a ligand binding profile that is different from its homolog in *P. aeruginosa* PAO1. A comparison of these results with previous studies of amino acid chemoreceptors emphasizes that even homologous chemoreceptors – such as the amino acid chemoreceptors from *P. aeruginosa* PAO1, *P. fluorescens* Pf0-1 and *Bacillus subtilis* – can have very different ligand binding profiles (Glekas *et al*., 2012; Oku *et al*., 2012; Rico-Jimenez *et al*., 2013). Together, this emphasizes the need for tractable experimental approaches to assess LBD binding profiles, rather than relying on inferences that are based on (comparatively low) levels of sequence identity.

Another important aspect of this study was the discovery that the *Psa* PscA-LBD can detect aspartate (Fig. 2A and Fig. 3). This is in stark contrast to any of the homologs from *P. aeruginosa* PAO1 – none of which detect aspartate or glutamate. The ability of a bacterium to detect and respond to specific chemicals in the environment can increase its chances of locating useful sources of carbon and energy. Therefore, it is possible that these differences reflect the different lifestyles of these *Pseudomonas* species. *Psa* has a narrow host range, only infecting green-and yellow-fleshed kiwifruit (Scortichini *et al*., 2012). In comparison, *P. aeruginosa* PAO1 is an almost ubiquitous environmental presence that can cause infections in a wide range of animals and plants. Acidic amino acids are the predominant amino acids found in plant exudates and can be utilized as a source of carbon, nitrogen and energy by many Pseudomonads (Sonawane *et al*., 2003). Logically, it follows that the ability to detect and navigate toward these amino acids may contribute to the capacity of *Psa* to detect and colonize its plant host. It will be interesting to explore

the roles of the remaining 30 chemoreceptor proteins of *Psa*, as this will provide important insights into how this bacterium recognizes its host.

Finally, our results demonstrated that a single amino acid mutation can dramatically alter the specificity of a chemoreceptor. The A146D mutation in the *Psa* PscA-LBD conferred the ability to recognize 14 new amino acids. Inspection of our structure-based alignment (Fig. S6) and comparison with other previously characterized amino acid chemoreceptors (Glekas *et al.*, 2012; Oku *et al.*, 2012; Rico-Jimenez *et al.*, 2013) suggests that the presence of an aspartate residue at this position precludes the binding of acidic ligands. In contrast, no obvious predictions about specificity can be made based on the presence of an alanine at this position. Currently, there are no structural data available for any of the *Pseudomonas* amino acid LBDs. Structures of the PctA-LBD from *P. aeruginosa*, and the PscA-LBD from *Psa*, will be highly informative for elucidating the molecular basis of their disparate specificities. Nevertheless, the results of this mutagenesis study demonstrate that single mutations can have large effects and provide direct experimental support for the hypothesis that chemosensing is a highly evolvable phenotype (Wuichet and Zhulin, 2003).

Experimental procedures

Materials

All enzymes for molecular biology were purchased from New England Biolabs (Ipswich, MA, USA). Oligonucleotides were from Integrated DNA Technologies (Coralville, IA, USA). Growth media were from ForMedium (Hunstanton, Norfolk, UK). Benzonase nuclease was from EMD Chemicals (San Diego, CA, USA). Talon metal affinity resin was from Clontech (Mountain View, CA, USA). Protease inhibitor cocktail, chicken egg white lysozyme and chemicals were from Sigma Chemical (St. Louis, MO, USA). Phenotype microarray plates were from Biolog (Hayward, CA, USA). SYPRO Orange protein dye was from Life Technologies (Carlsbad, CA, USA).

Strains, plasmids and culture conditions

Strains and plasmids used are shown in Table S2. *E. coli* and *P. aeruginosa* PAO1 were grown at 37°C, whereas *Psa* was grown at 28°C. Cultures were routinely propagated in Luria–Bertani (LB) broth.

Bioinformatics

Periplasmic regions of membrane-bound proteins were determined by predicting transmembrane regions using TOPCONS (Bernsel *et al.*, 2009). Functional domains of proteins were predicted using the NCBI Conserved Domain Search (Marchler-Bauer and Bryant, 2004) with default parameters. Structural predictions of the LBDs were performed using the Phyre2 server (Kelley and Sternberg, 2009).

Cloning and mutagenesis

All primers used are listed in Table S3. The DNA fragment of *P. aeruginosa* PAO1 *pctA* (locus ID 4309) encoding amino acids Asn30-Ala278 was amplified using Phusion polymerase (Thermo Fisher Scientific, Waltham, MA, USA) and the primers 806.for and 807.rev. The DNA fragment of the *Psa pscA* gene (locus ID 14525), encoding amino acids Tyr31-Thr276, was amplified from *Psa* strain ICMP 18884, using the primers 776.for and 777.rev. Similarly, the DNA fragment of *Psa pscB* (locus ID 08785), encoding PscB-LBD (Tyr30-Ser273), was amplified using the primers 808.for and 809.rev; and the *Psa pscC* (locus ID 18055) fragment encoding PscC-LBD (Val28-Trp293) was amplified using 810.for and 811.rev. The resulting PCR products were each cloned into the expression vector pET28(a+) using the appropriate restriction enzymes. To generate the PscA-LBD A146D mutant, the Quikchange II Site-Directed Mutagenesis Kit (Stratagene, La Jolla, CA, USA) was used with the primers 814.QC1 and 815.QC2. All constructs were verified by DNA sequencing. The resulting plasmids (pET28-*Pae*-PctA-LBD, pET28-*Psa*-PscA-LBD, pET28-*Psa*-PscB-LBD, pET28-*Psa*-PscC-LBD and pET28-*Psa*-PscA-A146D-LBD) were used to transform the expression host, *E. coli* strain BL21 GOLD (DE3).

Protein expression and purification

Cultures were grown at 37°C in phosphate buffered Terrific Broth containing kanamycin (30 μg ml^{-1}) to A_{600} ~ 0.8. The cultures were shifted to 18°C, protein expression was induced by the addition of IPTG (1 mM) and the cultures were incubated for an additional 20 h. Cells were harvested by centrifugation, and the pellets were stored at –80°C. The cell pellet (~4.0 g wet cell weight from 400 ml culture) was resuspended in 10 ml of lysis buffer (50 mM potassium phosphate, 300 mM NaCl, pH 7.0). Protease inhibitor cocktail (80 μl), Benzonase nuclease (0.4 μl at 25 U μl^{-1}) and lysozyme (0.5 mg ml^{-1}, final concentration) were added. After 20 min incubation at 4°C, cells were lysed by sonication on ice, and the lysates were clarified by centrifugation (21,000× *g*, 4°C, 30 min). The clarified lysate was mixed with 800 μl Talon metal affinity resin (50% w/v slurry), and the mixture was gently agitated at 4°C for 60 min to allow the His_6-tagged protein to bind the resin. The resin was washed twice with 10 bed volumes of lysis buffer, before being transferred to a gravity flow column. After two further washes with 5 bed volumes of lysis buffer containing 5 mM imidazole and 10 mM imidazole, respectively, the purified protein was eluted with elution buffer (50 mM potassium phosphate, 300 mM NaCl, and 150 mM imidazole, pH 7.0). For proteins used in thermal shift assays, Amicon Ultra centrifugal filter units (10 kDa molecular weight cutoff; Millipore, Billerica, MA, USA) were used to exchange the purified proteins into storage buffer (50 mM potassium phosphate, 200 mM NaCl, 10% glycerol, pH 7.5), and aliquots were snap-frozen in liquid nitrogen and stored at –80°C. For ITC experiments, the proteins were dialyzed exhaustively against the same storage buffer before snap-freezing; the final dialysis buffer was used to prepare the ligand solution(s). Protein concentrations were quantified by measuring A_{280}, using extinction coefficients calculated according to Pace *et al.* (1995).

Thermal shift assays

Thermal shift assays were performed using a Roche LightCycler 480 Real-Time PCR instrument. For high-throughput screening, ligands were prepared by dissolving Biolog PM compounds in 50 μl of water to obtain a final concentration of around 10–20 mM. Screening was performed with plate PM3B. Each plate contains 95 compounds and a water (no ligand) control. The complete plate contents are listed in Table S2.

Each 20 μl standard assay contained 10 μM protein and SYPRO Orange at 5× concentration in a buffer containing 50 mM potassium phosphate, 200 mM NaCl 10% glycerol, pH 7.5. Two microliters of the resuspended Biolog compounds were added to each well. Samples were heat denatured from 20°C to 80°C at a ramp rate of 1.2°C min^{-1}. The protein unfolding curves were monitored by detecting changes in SYPRO Orange fluorescence. The first derivative values (–dF/dt) from the raw fluorescence data were used to determine the melting temperature (T_m). For compounds with stabilizing effects in the range of 1–2°C, LBDs were rescreened in the presence of 0, 1, 5 and 10 mM of each potential ligand to confirm binding. The ligands were prepared as 10× stocks, 2 μl were added to each well and the experiments were conducted as described above. All experiments were performed in triplicate.

Isothermal titration calorimetry

All experiments were carried out using a VP-microcalorimeter (Microcal) at 25°C. Typically, 120 μM of protein was titrated with 10 μl injections of 0.6–2 mM ligand solutions that were prepared immediately before use in dialysis buffer. All measurements were made in triplicate, from independently purified batches of protein. The evolved heats were integrated and normalized for protein concentration to generate binding isotherms. These were baseline corrected by subtraction of data from control experiments where the same concentration of ligand was titrated into buffer. The baseline-corrected data were fitted by an equation for a single-site model (unless otherwise noted) using Origin ITC software supplied by Microcal.

Generation of P. aeruginosa ΔpctA

The unmarked gene deletion was constructed in *P. aeruginosa* PAO1 using gene splicing by overlap extension (SOE) PCR and two-step allelic exchange. First, a knockout construct was made by amplifying ~750 bp nucleotide regions that flank the *pctA* gene using the primer pairs: 972.for, 973.rev; and 974.for, 975.rev (Table S3). A third PCR reaction with primers 972.for and 975.rev was used to assemble the flanking sequences. The resulting ~1.6 kb deletion fragment was TA-cloned into pCR8/GW/TOPO (Invitrogen), confirmed by sequencing and then subcloned into the suicide vector pUIC3 (Rainey, 1999) using BamHI and SpeI. The method for introducing the resulting construct, pUIC3-Δ*pctA*, into *P. aeruginosa* PAO1, and then screening for colonies with the markerless Δ*pctA* mutation, has been described previously (Gerth *et al.*, 2012). The deletion was confirmed by PCR and DNA sequencing.

*Generation of Psa Δ*pscA

The unmarked gene deletion was constructed in *Psa* using gene SOE PCR and allelic exchange by homologous recombination. The deletion construct was made by amplifying ~750 bp nucleotide regions that flank the *pscA* gene (locus ID 14525) using the primer pairs: 956.for, 957.rev; and 958.for, 959.rev (Table S3). A third PCR reaction with primers 956.for and 959.rev was used to assemble the flanking sequences. The resulting ~1.6 kb deletion fragment was TA-cloned into pCR8/GW/TOPO (Invitrogen) and confirmed by sequencing. The fragment was then subcloned into pK18mobsacB (Schafer *et al.*, 1994) using Gibson assembly (Gibson *et al.*, 2009) with the following primers: 1055.rev and 1058.for; 1056.for and 1057.rev. The deletion construct, pK18mobsacB-FR-Psa14525, was introduced into *Psa* by conjugation. The recipient *Psa* strain was grown overnight at 28°C, then mixed with *E. coli* DH5α carrying pK18mobsacB-FR-Psa14525 (donor strain) and *E. coli* carrying pRK2013 (helper strain). Chromosomal integration of pK18mobsacB-FR-Psa14525 by a single homologous recombination event was selected by plating on LB agar containing kanamycin (30 μg ml^{-1}) and nitrofurantoin (100 μg ml^{-1}). Nitrofurantoin was used to counter-select the *E. coli* DH5α donor cells. In order to select for recombinants that have excised the vector, suspensions of KanR isolates were diluted and plated onto 10% (w/v) sucrose plates. Sucrose-resistant colonies were then screened for Kan sensitivity (indicating the expected loss of the pK18mobsacB-based construct), as well PCR analysis using primers situated outside the region of the locus where recombination occurred. The deletion was confirmed by PCR analysis and DNA sequencing.

Quantitative capillary chemotaxis assays. The quantitative capillary chemotaxis assays were carried out as described previously, with slight modifications (Rico-Jimenez *et al.*, 2013). Cultures of *P. aeruginosa* PAO1 were grown to early stationary phase in LB at 37°C. *Psa* was cultured in tryptone broth (1% tryptone and 0.5% NaCl) at 28°C. The cultures were harvested by centrifugation; the pellets were washed gently in chemotaxis buffer (10 mM potassium phosphate, 1 mM $MgCl_2$, 0.1 mM EDTA, pH 7.0), and then resuspended in the same buffer to an OD_{600} of ~0.1. One microliter capillary tubes (Drummond Scientific, Broomall, PA, USA) were sealed at one end and filled with either chemotaxis buffer alone (as a control), or chemotaxis buffer containing the indicated ligand at 1 mM. When cooled, the capillary was placed into the bacterial suspension and incubated. After the period of incubation (10 min for *P. aeruginosa* cultures, or 30 min for *Psa* cultures), the capillaries were removed from the cell suspension and washed. The contents were expelled into 1 ml of chemotaxis buffer, and dilutions were plated for colony counts on LB agar plates.

Acknowledgements

This research was supported by a grant from the University of Otago School of Medical Sciences Early Career Dean's Bequest Fund. We would like to thank Dr. Peter Fineran (University of Otago) for providing *Psa* NZ-V13 genomic DNA. We would also like to thank Dr. Matt Templeton (Plant

& Food Research) for providing us with the pK18mobsacB plasmid and for his advice on constructing the *Psa* Δ*pscA* strain.

References

Adler, J. (1966) Chemotaxis in bacteria. *Science* **153:** 708–716.

Adler, J. (1969) Chemoreceptors in bacteria. *Science* **166:** 1588–1597.

Alvarez-Ortega, C., and Harwood, C.S. (2007) Identification of a malate chemoreceptor in *Pseudomonas aeruginosa* by screening for chemotaxis defects in an energy taxis-deficient mutant. *Appl Environ Microbiol* **73:** 7793–7795.

Bernsel, A., Viklund, H., Hennerdal, A., and Elofsson, A. (2009) TOPCONS: consensus prediction of membrane protein topology. *Nucleic Acids Res* **37:** W465–W468.

Bochner, B.R., Gadzinski, P., and Panomitros, E. (2001) Phenotype microarrays for high-throughput phenotypic testing and assay of gene function. *Genome Res* **11:** 1246–1255.

Cimmperman, P., Baranauskiene, L., Jachimoviciute, S., Jachno, J., Torresan, J., Michailoviene, V., *et al*. (2008) A quantitative model of thermal stabilization and destabilization of proteins by ligands. *Biophys J* **95:** 3222–3231.

Gerth, M.L., Ferla, M.P., and Rainey, P.B. (2012) The origin and ecological significance of multiple branches for histidine utilization in *Pseudomonas aeruginosa* PAO1. *Environ Microbiol* **14:** 1929–1940.

Gibson, D.G., Young, L., Chuang, R.Y., Venter, J.C., Hutchison, C.A., 3rd, and Smith, H.O. (2009) Enzymatic assembly of DNA molecules up to several hundred kilobases. *Nat Methods* **6:** 343–345.

Giuliani, S.E., Frank, A.M., and Collart, F.R. (2008) Functional assignment of solute-binding proteins of ABC transporters using a fluorescence-based thermal shift assay. *Biochemistry* **47:** 13974–13984.

Glekas, G.D., Foster, R.M., Cates, J.R., Estrella, J.A., Wawrzyniak, M.J., Rao, C.V., and Ordal, G.W. (2010) A PAS domain binds asparagine in the chemotaxis receptor McpB in *Bacillus subtilis*. *J Biol Chem* **285:** 1870–1878.

Glekas, G.D., Mulhern, B.J., Kroc, A., Duelfer, K.A., Lei, V., Rao, C.V., and Ordal, G.W. (2012) The *Bacillus subtilis* chemoreceptor McpC senses multiple ligands using two discrete mechanisms. *J Biol Chem* **287:** 39412–39418.

Hazelbauer, G.L., Falke, J.J., and Parkinson, J.S. (2008) Bacterial chemoreceptors: high-performance signaling in networked arrays. *Trends Biochem Sci* **33:** 9–19.

Kato, J., Kim, H.E., Takiguchi, N., Kuroda, A., and Ohtake, H. (2008) *Pseudomonas aeruginosa* as a model microorganism for investigation of chemotactic behaviors in ecosystem. *J Biosci Bioeng* **106:** 1–7.

Kelley, L.A., and Sternberg, M.J. (2009) Protein structure prediction on the Web: a case study using the Phyre server. *Nat Protoc* **4:** 363–371.

Krell, T., Lacal, J., Munoz-Martinez, F., Reyes-Darias, J.A., Cadirci, B.H., Garcia-Fontana, C., and Ramos, J.L. (2011) Diversity at its best: bacterial taxis. *Environ Microbiol* **13:** 1115–1124.

Krishna, S.N., Luan, C.H., Mishra, R.K., Xu, L., Scheidt, K.A., Anderson, W.F., and Bergan, R.C. (2013) A fluorescence-based thermal shift assay identifies inhibitors of mitogen activated protein kinase kinase 4. *PLoS ONE* **8:** e81504.

Lacal, J., Alfonso, C., Liu, X., Parales, R.E., Morel, B., Conejero-Lara, F., *et al*. (2010a) Identification of a chemoreceptor for tricarboxylic acid cycle intermediates: differential chemotactic response towards receptor ligands. *J Biol Chem* **285:** 23126–23136.

Lacal, J., Garcia-Fontana, C., Munoz-Martinez, F., Ramos, J.L., and Krell, T. (2010b) Sensing of environmental signals: classification of chemoreceptors according to the size of their ligand binding regions. *Environ Microbiol* **12:** 2873–2884.

Lo, M.C., Aulabaugh, A., Jin, G., Cowling, R., Bard, J., Malamas, M., and Ellestad, G. (2004) Evaluation of fluorescence-based thermal shift assays for hit identification in drug discovery. *Anal Biochem* **332:** 153–159.

McCann, H.C., Rikkerink, E.H., Bertels, F., Fiers, M., Lu, A., Rees-George, J., *et al*. (2013) Genomic analysis of the Kiwifruit pathogen *Pseudomonas syringae* pv. *actinidiae* provides insight into the origins of an emergent plant disease. *PLoS Pathog* **9:** e1003503.

Marchler-Bauer, A., and Bryant, S.H. (2004) CD-Search: protein domain annotations on the fly. *Nucleic Acids Res* **32:** W327–W331.

Niesen, F.H., Berglund, H., and Vedadi, M. (2007) The use of differential scanning fluorimetry to detect ligand interactions that promote protein stability. *Nature Protoc* **2:** 2212–2221.

Oku, S., Komatsu, A., Tajima, T., Nakashimada, Y., and Kato, J. (2012) Identification of chemotaxis sensory proteins for amino acids in *Pseudomonas fluorescens* Pf0-1 and their involvement in chemotaxis to tomato root exudate and root colonization. *Microbes Environ* **27:** 462–469.

Pace, C.N., Vajdos, F., Fee, L., Grimsley, G., and Gray, T. (1995) How to measure and predict the molar absorption coefficient of a protein. *Protein Sci* **4:** 2411–2423.

Pantoliano, M.W., Petrella, E.C., Kwasnoski, J.D., Lobanov, V.S., Myslik, J., Graf, E., *et al*. (2001) High-density miniaturized thermal shift assays as a general strategy for drug discovery. *J Biomol Screen* **6:** 429–440.

Parales, R.E., Luu, R.A., Chen, G.Y., Liu, X., Wu, V., Lin, P., *et al*. (2013) *Pseudomonas putida* F1 has multiple chemoreceptors with overlapping specificity for organic acids. *Microbiology* **159:** 1086–1096.

Rahman, H., King, R.M., Shewell, L.K., Semchenko, E.A., Hartley-Tassell, L.E., Wilson, J.C., *et al*. (2014) Characterisation of a multi-ligand binding chemoreceptor CcmL (Tlp3) of *Campylobacter jejuni*. *PLoS Pathog* **10:** e1003822.

Rainey, P.B. (1999) Adaptation of *Pseudomonas fluorescens* to the plant rhizosphere. *Environ Microbiol* **1:** 243–257.

Rico-Jimenez, M., Munoz-Martinez, F., Garcia-Fontana, C., Fernandez, M., Morel, B., Ortega, A., *et al*. (2013) Paralogous chemoreceptors mediate chemotaxis towards protein amino acids and the non-protein amino acid gamma-aminobutyrate (GABA). *Mol Microbiol* **88:** 1230–1243.

Schafer, A., Tauch, A., Jager, W., Kalinowski, J., Thierbach, G., and Puhler, A. (1994) Small mobilizable multi-purpose cloning vectors derived from the *Escherichia coli* plasmids pK18 and pK19: selection of defined deletions in the chromosome of *Corynebacterium glutamicum*. *Gene* **145:** 69–73.

Scortichini, M., Marcelletti, S., Ferrante, P., Petriccione, M., and Firrao, G. (2012) *Pseudomonas syringae* pv. *actinidiae*: a re-emerging, multi-faceted, pandemic pathogen. *Mol Plant Pathol* **13:** 631–640.

Sonawane, A., Kloppner, U., Hovel, S., Volker, U., and Rohm, K.H. (2003) Identification of *Pseudomonas* proteins coordinately induced by acidic amino acids and their amides: a two-dimensional electrophoresis study. *Microbiology* **149:** 2909–2918.

Taguchi, K., Fukutomi, H., Kuroda, A., Kato, J., and Ohtake, H. (1997) Genetic identification of chemotactic transducers for amino acids in *Pseudomonas aeruginosa*. *Microbiology* **143:** 3223–3229.

Tajima, H., Imada, K., Sakuma, M., Hattori, F., Nara, T., Kamo, N., *et al*. (2011) Ligand specificity determined by differentially arranged common ligand-binding residues in bacterial amino acid chemoreceptors Tsr and Tar. *J Biol Chem* **286:** 42200–42210.

Tso, W.W., and Adler, J. (1974) Negative chemotaxis in *Escherichia coli*. *J Bacteriol* **118:** 560–576.

Wadhams, G.H., and Armitage, J.P. (2004) Making sense of it all: bacterial chemotaxis. *Nat Rev Mol Cell Biol* **5:** 1024–1037.

Webb, B.A., Hildreth, S., Helm, R.F., and Scharf, B.E. (2014) *Sinorhizobium meliloti* chemoreceptor McpU mediates chemotaxis toward host plant exudates through direct proline sensing. *Appl Environ Microbiol* **80:** 3404–3415.

de Weert, S., Vermeiren, H., Mulders, I.H., Kuiper, I., Hendrickx, N., Bloemberg, G.V., *et al*. (2002) Flagella-driven chemotaxis towards exudate components is an important trait for tomato root colonization by *Pseudomonas fluorescens*. *Mol Plant Microbe Interact* **15:** 1173–1180.

Winsor, G.L., Lam, D.K., Fleming, L., Lo, R., Whiteside, M.D., Yu, N.Y., *et al*. (2011) *Pseudomonas* Genome Database: improved comparative analysis and population genomics capability for *Pseudomonas* genomes. *Nucleic Acids Res* **39:** D596–D600.

Wuichet, K., and Zhulin, I.B. (2003) Molecular evolution of sensory domains in cyanobacterial chemoreceptors. *Trends Microbiol* **11:** 200–203.

Yao, J., and Allen, C. (2006) Chemotaxis is required for virulence and competitive fitness of the bacterial wilt pathogen *Ralstonia solanacearum*. *J Bacteriol* **188:** 3697–3708.

Supporting information

Additional supporting information may be found in the online version of this article at the publisher's web-site.

